Plasmon-Enhanced Refractometry Through Cladding Mode Excitation by a Fiber Bragg Grating in Photonic Crystal Fiber

Olga Rusyakina, Tigran Baghdasaryan, Karima Chah, Pawel Mergo, Hugo Thienpont, Christophe Caucheteur, Francis Berghmans, *Senior Member, IEEE*, and Thomas Geernaert

***Abstract*—We report on an extrinsic surface plasmon-enhanced refractometer based on cladding mode resonance excitation in a photonic crystal fiber (PCF) equipped with a straight fiber Bragg grating (FBG). First, we show that the lattice pitch and the air hole diameter of the PCF microstructure define the spectral location of the excited cladding mode resonances. Second, we demonstrate that if the PCF parameters are properly selected, those resonances are sensitive to increases in steps of 1×10^{-4} refractive index units (RIU) of the refractive index value close to that of water. To the best of our knowledge, this is the first time that the sensitivity of PCF cladding mode resonances to refractive index changes in water-based solutions is reported. We achieved experimental values of 40.3 nm/RIU in terms of wavelength sensitivity and −801 dB/RIU in terms of amplitude sensitivity. The performance of our sensor is therefore comparable to that of tilted FBGs in step-index fibers used for water refractometry, which indicates the potential of our PCF sensor for biosensing. In addition, the sensor fabrication does not require any post-processing such as etching or polishing, which allows preserving the integrity of the fiber probe. Finally, the narrow spectrum within which the PCF operates, allows envisaging multi-target detection with a single fiber probe by using cascaded wavelength-multiplexed gratings.**

Manuscript received June 30, 2021; revised September 27, 2021; accepted October 29, 2021. Date of publication November 4, 2021; date of current version February 16, 2022. This work was supported in part by Fonds Wetenschappelijk Onderzoek (FWO) under Grants G0F6218N (EOS-convention 30467715), 12P1720N, and I013918N; in part by Interreg under Grant NWE758 (Fotonica pilootlijnen); in part by Industrial Research Fund (IOF); in part by Methusalem; in part by the OZR of Vrije Universiteit Brussel; and in part by Fonds National de la Recherche Scientifique (F.R.S.-FNRS). Reference author: Olga Rusyakina. *(Corresponding author: Olga Rusyakina.)*

Olga Rusyakina is with Brussels Photonics (B-PHOT), Vrije Universiteit Brussel and Flanders Make, Dept. of Applied Physics and Photonics, Pleinlaan 2 1050, Brussels, Belgium, and also with the Department of Electromagnetism and Telecommunication, University of Mons, 31 Bld Dolez, 7000 Mons, Belgium (e-mail: olga.rusyakina@vub.be).

Tigran Baghdasaryan, Hugo Thienpont, Francis Berghmans, and Thomas Geernaert are with Brussels Photonics (B-PHOT), Vrije Universiteit Brussel and Flanders Make, Dept. of Applied Physics and Photonics, Pleinlaan 2 1050, Brussels, Belgium (e-mail: tbaghdas@b-phot.org; hugo.thienpont@vub.be; francis.berghmans@vub.be; thomas.geernaert@vub.be).

Karima Chah and Christophe Caucheteur are with the Department of Electromagnetism and Telecommunication, University of Mons, 31 Bld Dolez 7000, Mons, Belgium (e-mail: karima.chah@umons.ac.be; christophe.caucheteur@umons.ac.be).

Pawel Mergo is with the Laboratory of Optical Fibres Technology, Institute of Chemical Sciences, Maria Curie Sklodowska University, Sklodowska Sq. 3 20-031, Lublin, Poland (e-mail: pawel.mergo@poczta.umcs.lublin.pl).

Color versions of one or more figures in this article are available at https://doi.org/10.1109/JLT.2021.3125111.

Digital Object Identifier 10.1109/JLT.2021.3125111

***Index Terms*—Fiber bragg gratings, fiber optics sensors, photonic crystal fibers, refractive index measurement, surface plasmon resonance.**

I. Introduction

OPTICAL fiber technology has been widely considered for point-of-care diagnostics using so-called lab-on-fiber probes [1]–[3], which are often based on fiber Bragg grating (FBG) technology. Among various FBG-based sensors [4]–[6], one type that has shown to be particularly promising exploits tilted FBGs in standard step-index fibers [7]–[10]. Recent applications of tilted FBGs targeted *in situ* detection of cancerous human lung tissue with potential for *in vivo* measurements [11] and label-free sensing of breast cancer cells at ultra-low concentrations [12]. These applications exploit cladding mode resonances that are excited following the interaction of a forward-propagating fundamental core mode and the tilted grating inscribed in the fiber core [13]–[15]. The highest sensitivities are obtained for the resonance with an effective index that matches the refractive index (RI) of the analyte. Biomedical sensing therefore requires modes with effective indices close to the RI values of water, phosphate-buffered saline, or other cell culture media [16]. Since tilted FBGs in step-index fibers yield frequency combs that cover a broad spectrum, the choice of available modal effective indices and, therefore, the range of analytes that can be studied is wide. On the other hand, this also means that only a limited number of resonances with a specific effective index are sufficient to carry out a specific sensing task, whilst the other resonances do not show meaningful sensitivities and just consume the available spectral range of typical read-out devices.

The challenge to reduce the spectral width covered by broad frequency combs down to a few resonances of interest can be addressed by employing specialty fibers, such as photonic crystal fibers (PCFs). It is well known that the guiding properties of PCFs can be tuned by changing the lattice pitch and the air hole diameter [17]–[19], which makes them attractive for different applications including refractive index sensing [20] and biosensing [3], [21], [22]. However, many reports on PCF-based sensors were limited to numerical investigations [22], or involved post-processing procedures that would complicate their use in practice [23].

The majority of PCF-based refractometers use the fundamental core mode for sensing in view of accessing the highest

intensity of the evanescent field of the core mode. Two sensing approaches are commonly utilized in PCFs. The first approach employs filling of air voids of the PCF microstructure surrounding the core with an analyte (intrinsic sensing configuration). To achieve that, some probes require selective filling of air capillaries with the analyte [24]. Despite the high sensitivities that can be achieved owing to the proximity of the sensing region to the core mode, the calibration process with the required filling manipulations makes such sensors quite involved to work with and, therefore, make it challenging to proceed to the final biosensing applications.

The second approach is based on an extrinsic sensing configuration, which often requires modification of the fiber geometry by ways of mechanical polishing, tapering, etching or drilling, in order for the analyte to reach the PCF core region [25]–[27]. Whilst such extrinsic sensor architectures are easier to calibrate and reuse, and are hence preferred over intrinsic sensors [22], the required post-processing of such probes is time consuming, requires special equipment, may lead to probe-to-probe variation, and essentially also affects their mechanical integrity.

In view of improving the sensitivity, the fiber sensing region is also often covered with an additional functional layer to excite specific resonances. For example, excitation of lossy mode resonances requires metal oxide or polymer coatings [28], whilst surface plasmon resonances (SPR) are commonly excited in the presence of a thin (between 30 and 70 nm) layer of metal, mainly gold or silver. The SPR waves generated at the boundary between the metal layer and the surrounding medium, are highly sensitive to changes in the surrounding medium refractive index (SRI) [20]. Additionally, metal deposition is easier on the outer fiber surface of the extrinsic sensors than on the inside of the PCF air holes, which makes the extrinsic configurations advantageous over the intrinsic versions.

Sensing with PCF cladding mode resonances instead of the fundamental mode have been studied as well, but in a very limited number of cases [29]–[32]. Cladding mode resonances in hexagonal lattice PCFs excited following FBG inscription have been reported only by B. J. Eggleton *et al.* [29] and C. Chen *et al.* [32], with nearly zero sensitivity for an RI of 1.46 [29] and a maximal sensitivity of 12 nm/RIU for the resonances with the effective index matching the SRI in the range between 1.36 and 1.42 [32]. In both papers, the absence of cladding modes with an effective index matching the RI of water may be the reason for the low sensitivity in that SRI range, which in its turn renders such devices unfit for biosensing.

To compare the performance of various fiber refractometers, a figure of merit (FOM) defined as the ratio of the wavelength sensitivity to the full width at half maximum (FWHM) of the resonance is commonly adopted [8], [33], [34]. Numerical studies of plasmon-enhanced tilted FBGs in step-index fibers demonstrate high FOM values of $\sim$2500 RIU^{-1} calculated from the sensitivity of $\sim$500 nm/RIU obtained from the slope of wavelength shifts of all SPR resonances involved in sensing over a wide RI range of 1.30–1.44, divided by the sub-nanometer width of a single plasmon resonance responsible for sensing over a short RI range [35]. When tilted FBGs are experimentally applied to study small RI ranges of $\sim 1 \times 10^{-3}$ RIU, which are essential for biodetection, sensitivity calculations focus on a single resonance close to the SPR-attenuated region leading to wavelength sensitivities of $\sim$50–100 nm/RIU, and FOM values of $\sim$250–500 RIU^{-1} [36]–[38]. This approach has already shown great potential for the biodetection of cells [12], proteins [10], [36], and aptamers [39]. Another analysis method that uses the fitting of an envelope curve to the SPR-attenuated resonances, demonstrates sensitivities of a few hundred nm/RIU, with the nanometer wide envelopes resulting in lower FOM values of $\sim$50 RIU^{-1} [40], [41].

Plasmon-enhanced PCF-based refractometers have been applied to study wide RI ranges, in which they show high sensitivities of the order of $\sim 10^3$–10^4 nm/RIU, but limited FOM values of 100 RIU^{-1} due to the nanometer-level resonance widths [34]. The sensitivity across a large RI range is generally non-linear due to the index mismatch between the fundamental mode and the studied analyte, which especially affects the sensitivities at lower RI values such as water [2]. Therefore, although some PCF-based refractometers [34] and biosensors [42], [43] have been reported, the majority of the theoretically proposed PCF sensors still lack experimental demonstration.

The state-of-the-art reported above and the associated outstanding issues prompted us to investigate and develop a robust PCF-based RI sensor that:

- works in the extrinsic configuration whilst not requiring any post-processing of the fiber that would affect its geometry and mechanical integrity;
- displays resonances with effective index values close to the RI of water;
- is sensitive to RI changes of the order of $1\text{x}10^{-4}$ RIU of water-based solutions, and thus features potential for biosensing;
- is characterized by a high figure of merit enabled by the resonances with sub-nanometer FWHM values and the sensitivity values comparable to those of the most efficient fiber-based refractometers, in particular those using tilted FBGs in step-index fibers;
- operates in a narrow spectral region and can therefore be combined with multiple other probes by wavelength multiplexing the gratings within a single PCF.

The paper is further structured as follows: in section II, we describe the details of FBG inscription in two types of PCFs and analyze the cladding modes resonances revealed by their transmission spectra. Then, we focus on one of the two PCFs, for which we show the procedure for plasmon-enhanced water refractometry. For one of the polarizations that corresponds to the SPR-excited state, we show the detailed spectra of the sensing region after the PCF was immersed in seventeen RI solutions. In section III, we discuss the peculiarities of the plasmon-enhanced cladding mode excitation in PCFs, and we show that the proposed device is three times more sensitive than similar PCF-based configurations without metal layer [29], [32], and is comparable to state-of-the-art RI sensors in terms of the wavelength sensitivity and the FOM value. Finally, we summarize our results and briefly address perspectives for PCF-based grating-multiplexed sensing.

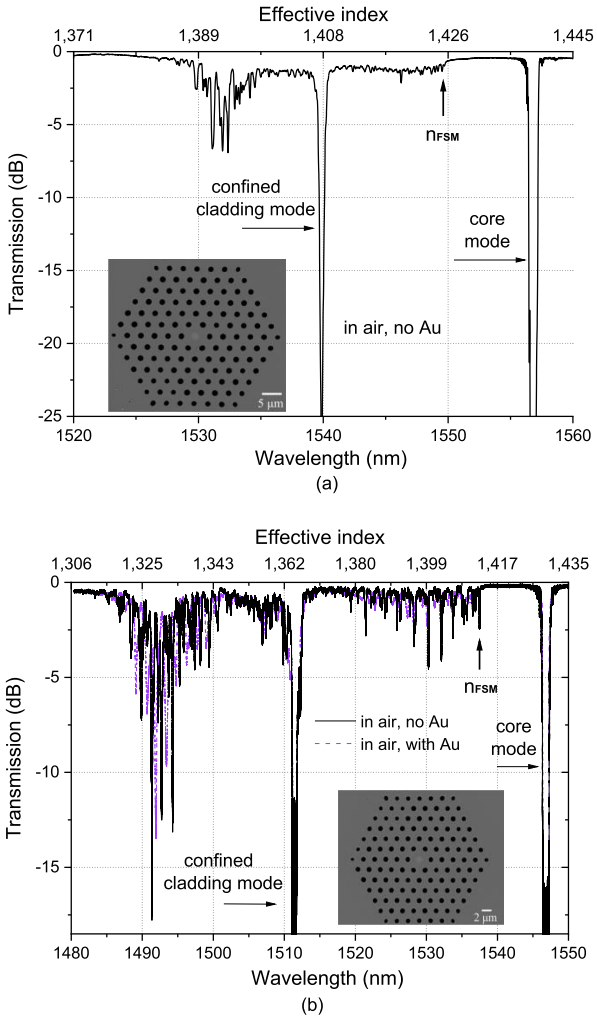

Fig. 1. Transmission spectra of straight FBGs inscribed in hexagonal lattice PCFs (micrographs of the cross-sections are shown in the insets) with an air-filling factor d/Λ = 0.4 and pitch values Λ = 3.6 μm (a) and 2.5 μm (b). For the PCF shown in (b), spectra are shown before (black) and after (dashed purple) gold deposition. The modes in the region 1490–1495 nm are used further in this work for SPR sensing in aqueous solutions.

II. Materials and Methods

We investigated two hexagonal lattice PCFs with six rings of air holes and cladding diameters of 125 and 86 μm [44]. The insets in Fig. 1 show the scanning electron microscope (SEM) images of the PCF microstructures in their cross-sections. Both PCFs have a core region doped with 8.5 mol% germanium. The lattice pitches are Λ = 3.6 and 2.5 μm and the air hole diameters are approximately equal to d = 1.4 and 1 μm, respectively. This yields an air-filling factor d/Λ of around 0.4 for both PCFs. Note that the diameter of the germanium doped portion of the core region is approximately equal to that of the air hole diameter for both fibers.

Before grating fabrication, the PCFs were hydrogen loaded at 60 °C for 60 hours at 205 bar to increase the photosensitivity. Straight fiber Bragg gratings were inscribed in both fiber samples using a 193 nm ArF excimer pulsed laser in a commercially available Noria FBG manufacturing station (NorthLab Photonics [45]). We wrote gratings with an average laser power of 250 mW, a repetition rate of 50 Hz, a pulse energy of 5 mJ, and a fluence at the photosensitive core of approximately 1.98 kW/cm^2 for the first and 2.8 kW/cm^2 for the second PCF. The period of the phase mask was $\Lambda_{\mathrm{PM}} = 1082$ nm (sourced from Ibsen Photonics [46]), resulting in a first-order FBG in the C-band with a period of $\Lambda_{\mathrm{FBG}} = \Lambda_{\mathrm{PM}}/2 = 541$ nm. After the photo-inscription, we annealed the fibers at 70 °C for 20 hours. The PCFs were spliced to conventional single-mode fiber pigtails using a Fujikura LZM-100 Laser Splicing System [47] to enable spectral interrogation in transmission.

A. FBG Transmission Spectra in PCFs

The transmission spectra of the straight FBGs (shown in Fig. 1) reveal the cladding mode excitations for both fibers. The resonances clearly feature different strengths and spectral positions. Such spectral responses of FBGs in hexagonal lattice PCFs are in agreement with those reported previously [29], [32], and have resonances with similar strengths. In [32], the authors showed simulated intensity profiles for the core and cladding mode resonances excited in the PCF as a result of FBG inscription.

We have previously shown that during grating writing in PCFs, complex interactions of the grating-writing laser beam with the holey cladding create a strongly non-uniform intensity distribution in the fiber cross-section, which results in non-uniform refractive index modifications in the core [48], [49]. The ability to excite cladding modes with straight FBGs in PCFs can be attributed to this non-uniformity. A similar mechanism is indeed responsible for the appearance of cladding mode resonances in the transmission spectra of some point-by-point [14] and eccentric gratings [50], [51] in step-index fibers, in which refractive index modifications are formed only in a limited region of the core. Note that our attempts to inscribe tilted FBGs in PCFs resulted in significantly weaker cladding resonances than the straight FBGs in the same PCFs.

Generally speaking, the PCF orientation in the inscription setup affects the index modulation in the core region. Our previous studies of laser-based inscription of FBGs in hexagonal lattice PCFs [48], [49], [52] showed that the PCF's microstructure with respect to the laser beam indeed causes a non-uniform index modulation across the core region, although it does not necessarily affect the average index modulation much. Hence, FBGs in PCFs can still yield strong core resonances. To check the reproducibility of the cladding mode resonances, we inscribed gratings into 15 PCF samples without controlling the fiber orientation during the inscription. The cladding modes in 10 PCF samples returned reproducible amplitude dips of 10 to 15 dB for the strongest cladding mode resonance. For the other 5 PCF samples, we observed weaker transmission dips of 4 to 7 dB. These differences most likely result from the influence of the fiber orientation in the inscription setup.

The number of cladding modes in the transmission spectra of PCFs with straight FBGs (Fig. 1) is relatively small compared to that in step-index fibers equipped with tilted FBGs [8], [9]. The PCF microstructure indeed limits the amount of the modes that can exist in the cladding. The microstructure geometry also

determines the spectral location of the cladding mode resonances with respect to the fundamental Bragg resonance and, therefore, their modal effective index. Since the air-filling factor is fixed for two PCF microstructures, the reason for specific spectral locations of the resonances originates from their different pitch values. Indeed, the lattice pitch change leads to variations in the modal intensity profile [31]. As a result, the spatial overlap of the modal intensity field with the microstructured cladding as well as with the medium outside the fiber, changes. Hence, the modal effective index also varies as a function of the lattice pitch [53]. Said effect of the geometry on the modal effective index can be supported by calculating the effective index of a fundamental space-filling mode n_{FSM} in a hexagonal lattice unit cell using COMSOL Multiphysics software [54]. The fundamental space-filling mode corresponds to the resonance with the maximal effective index allowed in the PCF microstructure. The values calculated for the PCFs shown in Fig. 1(a) and (b) are $n_{\mathrm{FSM}} = 1.428$ and $n_{\mathrm{FSM}} = 1.417$, respectively. These are very close to the measured values of 1.426 for PCF (a) and 1.412 for PCF (b), indicated in Fig. 1 with the arrows. The spectral distance between the core mode and the fundamental space-filling mode differs for the two fibers, which results from the difference in the pitch and the air hole diameter values.

Whether a PCF operates in a single-mode or multimode regime, can be assessed by considering the *V*-number given by [55]:

$$(2\pi\Lambda/\lambda) \cdot \left(\mathrm{n}_{\mathrm{FM}}^2 - \mathrm{n}_{\mathrm{FSM}}^2\right)^{1/2}, \tag{1}$$

with n_{FM} the effective index of the fundamental mode and n_{FSM} the effective index of the fundamental space-filling mode. These values can be obtained from the spectra shown in Fig. 1. The Bragg resonance that corresponds to the reflected fundamental core mode is centered around λ_{FM}, which gives an effective index $\mathrm{n}_{\mathrm{FM}} = \lambda_{\mathrm{FM}} / (2 \cdot \Lambda_{\mathrm{FBG}}) = 1.439$ for PCF (a), and $\mathrm{n}_{\mathrm{FM}} = 1.430$ for PCF (b). The calculated *V*-numbers are therefore ∼2.85 for PCF (a), and ∼2.27 for PCF (b). Values of *V* smaller than π correspond to a single-mode guidance regime [55], and hence both PCFs are clearly endlessly single-mode.

The strong resonances at 1540 nm for PCF (a), and at 1511 nm for PCF (b) correspond to the cladding modes confined in the core that show a negligible sensitivity to the surrounding RI. Similar resonances have been reported in literature and were attributed to cladding modes with most of their power concentrated in the core and within the two-three inner rings of the microstructure, resulting in a high overlap with both the fundamental mode and the grating perturbations [29], [32].

The spectrum in Fig. 1(a) reveals other cladding mode resonances in the wavelength region 1530–1535 nm. These resonances correspond to effective index values between 1.389–1.398, as calculated from the (2) for the effective index of any cladding mode coupled via a straight FBG given by:

$$\mathrm{n}_{\mathrm{eff,\ cladding}} = \left(\lambda_{\mathrm{cladding}}/\Lambda_{\mathrm{FBG}}\right) - \mathrm{n}_{\mathrm{FM}}, \tag{2}$$

where $\lambda_{\mathrm{cladding}}$ is the wavelength of the corresponding resonance in the transmission spectrum. The second PCF shows two regions with strong cladding mode resonances located in the spectrum on either side of the resonance at 1511 nm. The region 1519–1537 nm corresponds to the modes with effective index values between 1.379 and 1.413. The resonances from the region 1490–1495 nm have effective index values between 1.322 and 1.344 which are very close to the RI of water. Therefore, we will only use PCF (b) for refractometry in water-based solutions described below.

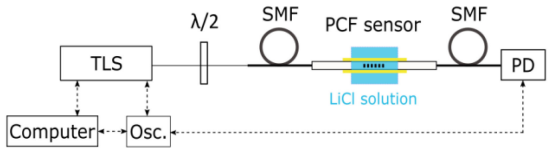

Fig. 2. Scheme of the experimental setup for SRI measurements. The PCF sensor is immersed in lithium chloride (LiCl) salt solutions. The read-out equipment consists of a tunable laser source (TLS), a half-waveplate (λ/2), an oscilloscope (Osc.), and a photodetector (PD).

To exploit surface plasmon resonance excitation, we deposited a layer of gold with a thickness of ∼35 nm using a sputter-coater chamber with argon at a pressure of 10^{-4} mbar (Leica EM SCD 500). This thickness was found to be an optimal value for tilted FBGs in single-mode fiber SPR refractometers [56]. The transmission spectrum of the gold-coated PCF (b) in air is shown with a dashed purple line in Fig. 1(b). Gold deposition reduced the strength of the transmission resonances with several dBs (∼6 dB for the strongest resonance from the wavelength span 1490-1495 nm). The external position of the gold layer allows for realization of an extrinsic sensing configuration which has an advantage of simpler calibration (and later, surface bio-functionalization) compared to the internally filled PCF-based sensors.

B. Plasmon-Enhanced Refractive Index Sensing With a PCF

For the refractive index sensing experiments, we prepared anhydrous lithium chloride salt (LiCl) dissolved in distilled water at seventeen different concentrations. The RI value of each solution was measured at 436.6 nm using an Abbemat MW refractometer with a resolution of 10^{-6} RIU. The RI difference between the solutions was around $1\text{x}10^{-4}$ RIU. We applied a Sellmeier fit for distilled water [57] to extrapolate the RI values to 1550 nm, resulting in the following values (limited to the fifth decimal): 1.31582, 1.31593, 1.31602, 1.31612, 1.31622, 1.31633, 1.31642, 1.31653, 1.31672, 1.31703, 1.31713, 1.31723, 1.31733, 1.31743, 1.31752, 1.31763, and 1.31773. The index of distilled water at 1550 nm was extrapolated to be 1.31495.

For the RI sensitivity measurements, the PCF sample was fixed using two fiber clamps with the grating held straight in a small reservoir. We added RI solution to the reservoir until the grating was completely covered with the liquid and then recorded the transmission spectrum. In between successive RI measurements, we rinsed the grating with distilled water and recorded the transmission spectrum in air to ensure that the sensor had returned to its initial state.

Fig. 2 shows the experimental setup. A tunable laser source (TLS) Santec TSL-710 was programmed to make a wavelength

sweep between 1480 and 1550 nm in steps of 0.6 pm at a tuning speed of 60 nm/s. The transmitted power was recorded with a Thorlabs PDA20CS photodetector (PD) with a built-in trans-impedance amplifier. An oscilloscope (Osc.) was synchronized with the wavelength-swept system and the PD output to retrieve the transmission spectrum. We used a MATLAB script to control the setup and record the spectrum. The linear polarization angle of the laser source was controlled using a half-waveplate (λ/2). After recording the transmission spectra of the PCF immersed in all RI solutions, we processed the data in MATLAB by tracking the wavelength and the intensity level of all the dips in the transmission spectra. The resonances in the wavelength range 1488-1500 nm generally showed larger sensitivities than the resonances from the rest of the spectrum. The proximity of effective indices to the refractive index of water allows them to fulfil the phase matching condition to couple to the SPR wave. On the other hand, the modal field distributions that extend up to the cladding boundary, allow obtaining the largest wavelength and amplitude shifts as a response to the varying external index. A detailed discussion of the most sensitive resonances is given in section III.

C. Temperature Dependence of the PCF Cladding Modes

Fiber-based RI sensors are known to exhibit cross-sensitivity to temperature changes, which therefore affect the RI measurements. A priori knowledge of the modal sensitivity to temperature changes allows correcting the final RI measurements for spectral shifts due to temperature variations.

To perform the temperature calibration, we immersed the gold-coated FBG-equipped PCF in a temperature-controlled bath filled with distilled water. The immersion allows for a stable and uniform temperature and avoids air circulation that may affect the measurement accuracy. In addition, this situation mimics the actual conditions for our target RI sensing experiments as the fiber probe will be immersed in aqueous solutions. Temperature control and monitoring was enabled by placing the bath on a hot plate (Torrey Pines Scientific HS40) and measuring the temperature with an external needle-type digital thermometer (IKA ETS-D5) with a resolution of 0.1 °C placed next to the grating. Fig. 3 shows the resulting wavelength shifts for four resonances in the transmission spectrum for temperatures between 19 up to 40 °C. The core mode in our PCF has the highest temperature sensitivity of 9.3 pm/°C. This value is close to the values for straight FBGs in PCFs that have already been reported [32], [58]. Note that because this mode is highly confined in the core region, it is not affected by any index changes in the surrounding medium [8], [32]. Therefore, the spectral shift of the core mode is solely due to temperature variations in the surrounding medium.

Modes that are less confined in the core region are affected by changes in both temperature and external index. The confined cladding mode has a slightly lower thermal sensitivity of 9.0 pm/°C but close to that of the core mode. This mode is partially affected by the surrounding index due to leakage of the optical power in the mode through the microstructure to the interface between fiber and surrounding medium [32]. Modes 1 and 2 that we exploit for SPR sensing in aqueous solutions (a detailed description of these modes is provided further down the manuscript, including Figs. 4–6) show even lower sensitivity to temperature. In addition to an intrinsic thermal sensitivity, these modes are strongly influenced by the thermo-optic coefficients of water and gold. Whereas the effect of temperature changes on the permittivity of gold is small [59], distilled water features a large negative thermo-optic coefficient of approximately -1.4×10^{-4} RIU/°C [60], which lowers the slope of the temperature sensitivity line for modes 1 and 2. Study of other PCF samples (both with and without a gold coating) immersed in water showed that generally the resonances with an effective index value around the refractive index of water demonstrate temperature sensitivities that are ∼20–25% smaller than that of the core mode.

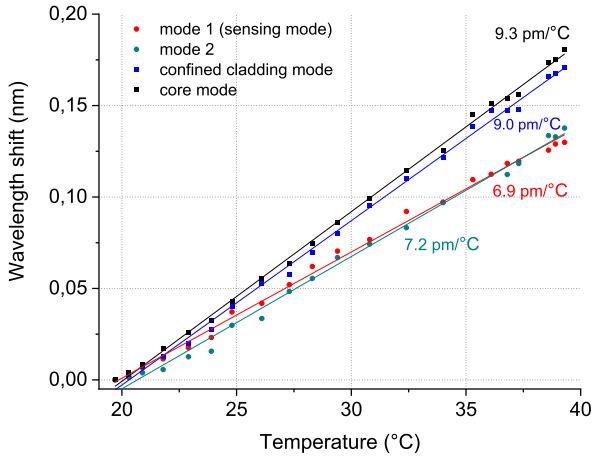

Fig. 3. Resonance wavelengths for selected modes show different dependencies on temperature variations in water. The core mode that is insensitive to the RI changes in the surrounding medium, shows the highest temperature sensitivity. Mode 1, which is most sensitive to the RI of the surrounding medium in aqueous solutions, features the lowest temperature sensitivity.

Although we carried out refractive index measurements with the PCF probe at room temperature, small fluctuations in the temperature still affected the experiments. We noticed picometer spectral shifts of the core resonance. Nevertheless, self-referencing to the core resonance together with the temperature sensitivities of the modes shown in Fig. 3 allowed to correct for those fluctuations.

III. Results and Discussion

Usually, only *p*-polarized light leads to the SPR excitation and to the highest sensitivity for tilted FBGs in step-index fibers [8]. To obtain the polarization state that resulted in the resonances with the largest spectral shift and amplitude change for this sensor configuration, we rotated the input polarization with the half-waveplate (λ/2) and carried out measurements in the set of RI solutions for several polarization angles. Fig. 4(a) shows the PCF transmission spectra measured when the input polarization is optimized for the SPR excitation (pol 1, red curve), and when the polarization orthogonal to the first one is considered (pol 2, black curve).

Fig. 4(b) shows transmission spectra of the grating immersed in the set of refractive index solutions, at the SPR-optimized

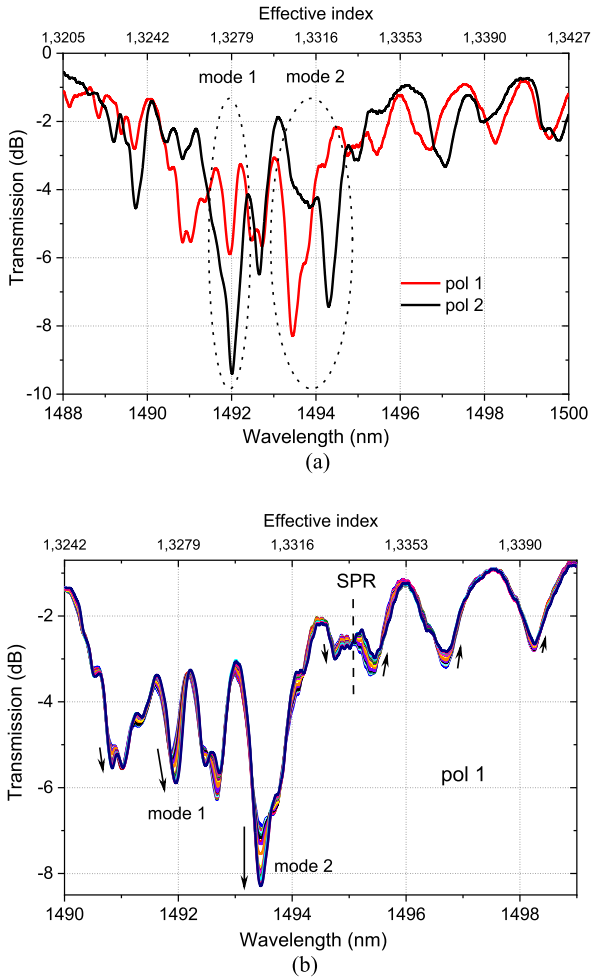

Fig. 4. (a) Transmission spectra of the grating in the gold-coated PCF at the input polarization optimized for the SPR excitation (pol 1, red) and at the polarization orthogonal to pol 1 (pol 2, black). Modes 1 and 2 indicated with the dotted lines correspond to the cladding mode resonances with the highest wavelength and amplitude sensitivity (see Figs. 5 and 6). (b) Transmission spectra of the gold-coated PCF grating after immersion in seventeen refractive index solutions at the SPR-optimized polarization. The dashed line indicates the position of the SPR-attenuated mode.

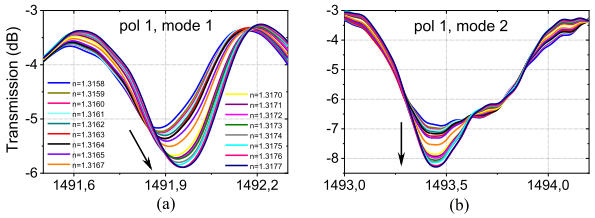

Fig. 5. Transmission spectra of modes 1 and 2 after immersion of the gold-coated PCF grating in seventeen refractive index solutions. The modes show the largest wavelength (a) and amplitude (b) shifts in the SPR-excited state.

polarization. The mode at 1495 nm indicated with a dashed line shows a behavior similar to that of the plasmonic modes in tilted FBGs [12]. When the gold layer is introduced, resonances with a specific effective index are phase-matched to the plasmonic waves and, as a result, are attenuated in the transmission spectrum. The plasmon-coupled area is then easily spotted as a region

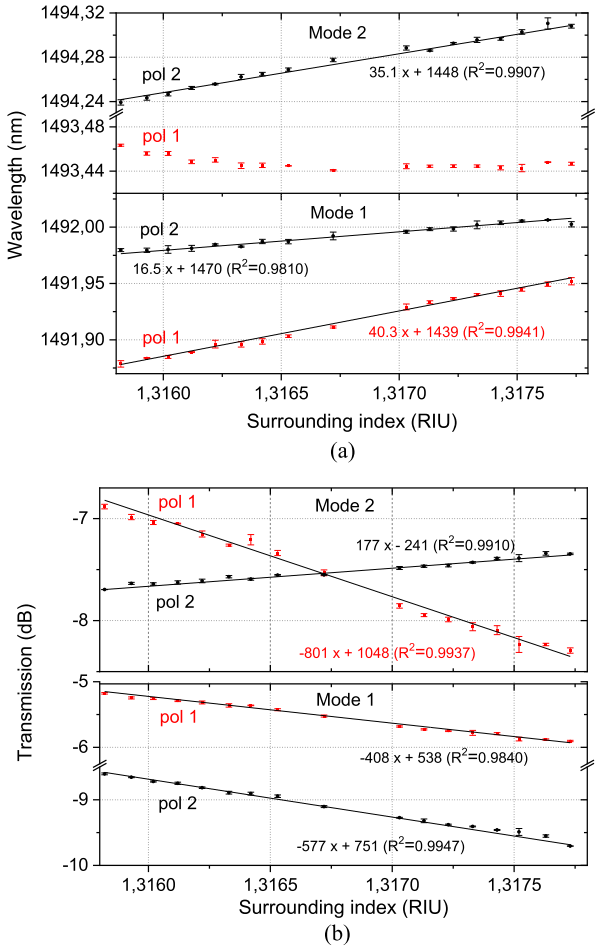

Fig. 6. Wavelength (a) and amplitude (b) sensitivity of modes 1 and 2, calculated from the linear fits (black lines) applied to Gaussian-fitted inverted resonance dips as a function of SRI values. Sensitivities for the modes in two orthogonal polarization states (pol 1, pol 2) are calculated. The error bars correspond to one standard deviation for three repeated measurements with the PCF refractometric probe immersed in the same RI solution.

of modes with sharply decreased amplitudes, as is the region around 1495 nm for our PCF. When the incident polarization is optimized for the SPR excitation, the resonances on the side of the shorter/longer wavelengths from the SPR mode show a peak-to-peak amplitude increase/decrease as a function of the increasing SRI value [12], which is shown with the arrows in Fig. 4(b). Similarly to what has been reported for tilted FBGs [12], [36], [61], the resonance wavelength located just below the plasmon-attenuated region, is the one that is the most affected by the amplitude changes induced by the SPR excitation. This mode (labelled 'mode 2' and indicated in Fig. 4(a) with a dotted line) experiences the most significant peak-to-peak amplitude change under variations in the external index. The mode with the largest wavelength shift (this is the mode labelled 'mode 1') is positioned at 1492 nm, i.e., a few nanometers below the SPR-attenuated mode what is also characteristic for tilted FBGs. The effective index of mode 1 calculated from equation (2) is $n_{eff} = 1.328$, which is slightly larger than that of the medium under test, which is another similarity to the approach using SPR-enhanced sensing with tilted FBGs [35].

Fig. 5 shows the behavior of modes 1 and 2 for the SPR-optimized polarization in a narrower wavelength range, after smoothening the spectra with a Savitzky–Golay filter [62]. The small changes of the order of $1\text{x}10^{-4}$ RIU in the surrounding index result in small differences between the spectra and hence in spectral shifts of a few picometers. The black arrows indicate the direction of the spectral shift of the resonance wavelength and of the resonance loss with increasing SRI values. To extract both wavelength and amplitude values, these transmission dips were inverted to obtain peaks instead of dips, and the tip of every peak was fitted with a Gaussian curve in view of applying a peak search algorithm. The slopes of the linear regression equations applied to the wavelength/amplitude varying as a function of the SRI values in Fig. 6, result in the sensitivity values as shown for modes 1 and 2 and for both polarizations. The error bars in Fig. 6 refer to $\pm$'one σ' standard deviation from the mean values obtained after three repeated measurements when the grating is immersed in the same RI solution.

At the SPR-optimized polarization 1, mode 1 shows the highest wavelength sensitivity of 40.3 nm/RIU with a linear fit with $R^2 = 0.9941$, Fig. 6(a). On the other hand, the wavelength of mode 2 does not follow a linear trend but features the highest amplitude shift with a slope of -801 dB/RIU ($R^2 = 0.9937$), Fig. 6(b). Polarization 2 excites the orthogonal polarization of both modes 1 and 2 (as also shown in Fig. 4(a)) leading to a red-shift in their spectral positions, Fig. 6(a). For the orthogonal polarization, mode 1 has a smaller sensitivity of 16.5 nm/RIU, whereas for mode 2 this is 35.1 nm/RIU. For the intermediate polarization states between two orthogonal polarizations, both modes 1 and 2 deliver values of wavelength and amplitude sensitivities that lie in between the values reported in Fig. 6 for pol1 and pol2. Thus, when the incident polarization angle is changed in the range between 0° and 360°, excitation of the most sensitive modes (with the corresponding largest sensitivities) is periodically repeated over 180°.

Non-zero sensitivities for the orthogonal polarization might originate from the fact that the FBG inscribed in the PCF is not tilted. Unlike tilted FBGs that lead to an ideal break in the cylindrical symmetry and, as a result, uniquely defined *p*- and *s*-polarizations [8] with the maximal/zero sensitivity for the *p*-/ *s*-polarization, our PCF sensor does not appear to have a polarization state with zero sensitivity. Resonance modes for tilted FBGs in regular step-index fibers can be grouped into families within which all the resonances show similar polarization and intensity distributions [63]. In PCFs, however, the modes do not demonstrate the same polarization, as can be seen in Fig. 4(b). However, modes 1 and 2 show maximally available amplitude dips in both polarizations pol 1 and pol 2. Considering that these two modes yield the highest sensitivities among all the resonances for the input polarization states within 90° (including pol 1, pol 2, and intermediate polarization states), we confirm that the polarization pol 1 provides the most sensitive SPR response available for the proposed probe configuration.

For comparison between non-SPR and SPR sensing configurations, we have observed that PCF samples without a gold layer result in a decrease of the wavelength sensitivity by $\sim$15% and of the amplitude sensitivity by $\sim$50% (in absolute value). Implementing a gold film thus mostly affects the modal amplitude sensitivity. In non-coated PCF samples, all the resonances from the sensing spectral region demonstrate positive amplitude shifts as a function of an increasing refractive index outside the fiber. After a gold layer is introduced, the modal amplitude behavior changes. Some resonances experience an increase in the amplitude level with an external index increment, resulting in negative amplitude shifts. These modes are reported with the maximal amplitude sensitivities in the SPR configuration.

The wavelength sensitivity of 35.4 $\pm$ 9.2 nm/RIU (standard deviation) was obtained from ten gold-coated PCF samples in which one straight first-order FBG was inscribed using the phase mask with the period of Λ_{PM}= 1082 nm, without controlling the PCF orientation during inscription. The FOM calculated for resonance 1 with the FWHM of 260 pm (in pol 1) is 157 RIU^{-1} which is of the same order of magnitude as for plasmon-enhanced tilted FBGs, but higher than the values reported for other PCFs that have been considered for water refractometry so far [20], [34]. The resolution of our PCF-based refractometer is $1.02\text{x}10^{-4}$ RIU, as calculated using the approach given in [64], which is comparable to the value of 10^{-4} RIU reported for tilted FBGs in regular step-index fibers [8].

IV. Conclusion

This paper shows a practical application of hexagonal lattice photonic crystal fiber for refractometry in water-based solutions. In contrast to other PCF-based refractometers, we do not apply any post-processing to the fiber (such as etching or polishing) to preserve the fiber's integrity. The fabrication of our probe consists of the inscription of straight instead of tilted fiber Bragg gratings, and of the deposition of a gold layer on the outer surface of the fiber cladding. An extrinsic sensing configuration allows for simple calibration and reuse of the fiber sensor which becomes much more challenging for intrinsic PCF-based devices. For the first time to our knowledge, we show the excitation of PCF cladding mode resonances with effective index values close to the refractive index of water, which enables refractometry in aqueous solutions. Our plasmonic PCF sensor is clearly sensitive to changes of the RI of aqueous solutions in steps of 10^{-4} RIU, with maximal wavelength and amplitude sensitivities of 40.3 nm/RIU and -801 dB/RIU, and a linearity better than 99%. The performance in terms of sensitivity, FWHM, FOM, and resolution is comparable to that of tilted FBGs in step-index fibers used for sensing of water RI increments of the order of 10^{-4} RIU [38], [56], [65], and for biosensing [37]. Both sensing mechanisms (wavelength and amplitude) are exploited in literature to estimate the performance of refractive index sensors and both have their own strengths and weaknesses. In general, the amplitude sensitivity is more likely to be affected by power fluctuations of the light source. Wavelength shifts typically do no suffer from power fluctuations and are therefore often preferred. Our sensitivity of 40.3 nm/RIU is 3.4 times larger than that for FBG-excited cladding modes in a non-plasmonic architecture with different lattice pitch/air hole diameter values [32]. The PCFs studied here also evidence that the features of the microstructure largely influence the spectral position and

spectral separation of the cladding modes, as also indicated in previous reports [29], [32]. This suggests that PCFs with even higher sensitivities can be obtained.

The applicability of tilted FBGs in step-index fibers for RI sensing in low index analytes such as water [8] or gases [66] is also limited by the width of their spectra that extends over tens of nanometers. The narrow spectral widths offered by PCFs allow envisaging multi-target sensing by ways of wavelength multiplexed FBGs cascaded within a single fiber probe [67]. The use of multiplexed gratings would indeed open possibilities for simultaneous measurements of different analytes/biomarkers, for ensuring measurement repeatability and improving accuracy, or for including reference measurements.

Disclosures. Patent application entitled "Microstructured optical fiber sensing device" GB2015547.9 was filed on September 30, 2020.

References

[1] P. Vaiano *et al.*, "Lab on fiber technology for biological sensing applications," *Laser Photon. Rev.*, vol. 10, no. 6, pp. 922–961, Nov. 2016.

[2] F. Chiavaioli, C. Gouveia, P. Jorge, and F. Baldini, "Towards a uniform metrological assessment of grating-based optical fiber sensors: From refractometers to biosensors," *Biosensors*, vol. 7, no. 4, Jun. 2017, Art. no. 23.

[3] S. Tabassum and R. Kumar, "Advances in fiber-optic technology for point-of-care diagnosis and in vivo biosensing," *Adv. Mater. Technol.*, vol. 5, no. 5, May 2020, Art. no. 1900792.

[4] D. L. Presti *et al.*, "Fiber Bragg gratings for medical applications and future challenges: A review," *IEEE Access*, vol. 8, pp. 156863–156888, 2020.

[5] F. Esposito *et al.*, "Long period grating in double cladding fiber coated with graphene oxide as high-performance optical platform for biosensing," *Biosens. Bioelectron.*, vol. 172, Art. no. 112747, Jan. 2021.

[6] A. Bekmurzayeva *et al.*, "Etched fiber Bragg grating biosensor functionalized with aptamers for detection of thrombin," *Sensors*, vol. 18, no. 12, Dec. 2018, Art. no. 4298.

[7] Y. Y. Shevchenko and J. Albert, "Plasmon resonances in gold-coated tilted fiber Bragg gratings," *Opt. Lett.*, vol. 32, no. 3, Feb. 2007, Art. no. 211.

[8] J. Albert, L.-Y. Shao, and C. Caucheteur, "Tilted fiber Bragg grating sensors," *Laser Photon. Rev.*, vol. 7, no. 1, pp. 83–108, Jan. 2013.

[9] T. Guo, "Fiber grating-assisted surface plasmon resonance for biochemical and electrochemical sensing," *J. Light. Technol.*, vol. 35, no. 16, pp. 3323–3333, Aug. 2017.

[10] J. Lao *et al.*, "Gold nanoparticle-functionalized surface plasmon resonance optical fiber biosensor: In situ detection of thrombin with 1 n·M detection limit," *J. Lightw. Technol.*, vol. 37, no. 11, pp. 2748–2755, Jun. 2019.

[11] M. Loyez *et al.*, "In situ cancer diagnosis through online plasmonics," *Biosens. Bioelectron.*, vol. 131, Dec. 2018, pp. 104–112, Apr. 2019.

[12] M. Loyez *et al.*, "Rapid detection of circulating breast cancer cells using a multiresonant optical fiber aptasensor with plasmonic amplification," *ACS Sensors*, vol. 5, no. 2, pp. 454–463, Feb. 2020.

[13] T. Erdogan and J. E. Sipe, "Tilted fiber phase gratings," *J. Opt. Soc. Amer. A*, vol. 13, no. 2, Feb. 1996, Art. no. 296.

[14] J. Thomas *et al.*, "Cladding mode coupling in highly localized fiber Bragg gratings: Modal properties and transmission spectra," *Opt. Exp.*, vol. 19, no. 1, Jan. 2011, Art. no. 325.

[15] A. Bialiayeu, A. Ianoul, and J. Albert, "Polarization-resolved sensing with tilted fiber Bragg gratings: Theory and limits of detection," *J. Opt.*, vol. 17, no. 8, Aug. 2015, Art. no. 085601.

[16] V. T. Hoang *et al.*, "Optical properties of buffers and cell culture media for optofluidic and sensing applications," *Appl. Sci.*, vol. 9, no. 6, Mar. 2019, Art. no. 1145.

[17] S. Biswas, R. S. Rafi, M. A. Al-Amin, and S. Alam, "Analysis of the effect of air hole diameter and lattice pitch in optical properties for hexagonal photonic crystal fiber," *Opt. Photon. J.*, vol. 5, no. 7, pp. 227–233, 2015.

[18] A. M. R. Pinto and M. Lopez-Amo, "Photonic crystal fibers for sensing applications," *J. Sensors*, vol. 2012, pp. 1–21, 2012.

[19] K. Saitoh and M. Koshiba, "Numerical modeling of photonic crystal fibers," *J. Lightw. Technol.*, vol. 23, no. 11, pp. 3580–3590, Nov. 2005.

[20] D. J. J. Hu and H. P. Ho, "Recent advances in plasmonic photonic crystal fibers: Design, fabrication and applications," *Adv. Opt. Photon.*, vol. 9, no. 2, Jun. 2017, Art. no. 257.

[21] Y. Zhao, Z. Deng, and J. Li, "Photonic crystal fiber based surface plasmon resonance chemical sensors," *Sensors Actuators B Chem,* vol. 202, pp. 557–567, Oct. 2014.

[22] I. Danlard and E. K. Akowuah, "Assaying with PCF-based SPR refractive index biosensors: From recent configurations to outstanding detection limits," *Opt. Fiber Technol.*, vol. 54, Jan. 2020, Art. no. 102083.

[23] S. C. Xue, R. I. Tanner, G. W. Barton, R. Lwin, M. C. J. Large, and L. Poladian, "Fabrication of microstructured optical fibers-Part II: Numerical modeling of steady-state draw process," *J. Lightw. Technol.*, vol. 23, no. 7, pp. 2255–2266, Jul. 2005.

[24] O. Rusyakina *et al.*, "Selective liquid filling of photonic crystal fibers using two-photon polymerization lithography without post-exposure development," *Micro-Structured Specialty Opt. Fibres VI*, no. April, 2020, Art. no. 28.

[25] X. Yu *et al.*, "Plasmonic enhanced fluorescence spectroscopy using side-polished microstructured optical fiber," *Sensors Actuators, B Chem,* vol. 160, no. 1, pp. 196–201, 2011.

[26] Y. Zhu, Z. He, and H. Du, "Detection of external refractive index change with high sensitivity using long-period gratings in photonic crystal fiber," *Sensors Actuators B Chem,* vol. 131, no. 1, pp. 265–269, Apr. 2008.

[27] L. Rindorf, J. B. Jensen, M. Dufva, L. H. Pedersen, P. E. Høiby, and O. Bang, "Photonic crystal fiber long-period gratings for biochemical sensing," *Opt. Exp.*, vol. 14, no. 18, 2006, Art. no. 8224.

[28] F. Chiavaioli and D. Janner, "Fiber optic sensing with lossy mode resonances: Applications and perspectives," *J. Lightw. Technol.*, vol. 39, no. 12, pp. 3855–3870, Jun. 2021.

[29] B. J. Eggleton, P. S. Westbrook, C. A. White, C. Kerbage, R. S. Windeler, and G. L. Burdge, "Cladding-mode-resonances in air-silica microstructure optical fibers," *J. Lightw. Technol.*, vol. 18, no. 8, pp. 1084–1100, Aug. 2000.

[30] O. V. Ivanov, S. A. Nikitov, and Y. V. Gulyaev, "Cladding modes of optical fibers: Properties and applications," *Phys.-Uspekhi*, vol. 49, no. 2, 2006, Art. no. 167.

[31] X. Jiang, Z. Gu, and L. Zheng, "Cladding modes in photonic crystal fiber: Characteristics and sensitivity to surrounding refractive index," *Opt. Eng.*, vol. 55, no. 1, Jan. 2016, Art. no. 017106.

[32] C. Chen, A. Laronche, G. Bouwmans, L. Bigot, Y. Quiquempois, and J. Albert, "Sensitivity of photonic crystal fiber modes to temperature, strain and external refractive index," *Opt. Exp.*, vol. 16, no. 13, Jun. 2008, Art. no. 9645.

[33] P. Offermans *et al.*, "Universal scaling of the figure of merit of plasmonic sensors," *ACS Nano*, vol. 5, no. 6, pp. 5151–5157, Jun. 2011.

[34] A. Urrutia, I. Del Villar, P. Zubiate, and C. R. Zamarreño, "A comprehensive review of optical fiber refractometers: Toward a standard comparative criterion," *Laser Photon. Rev.*, vol. 13, no. 11, Nov. 2019, Art. no. 1900094.

[35] C. Caucheteur, V. Voisin, and J. Albert, "Near-infrared grating-assisted SPR optical fiber sensors: Design rules for ultimate refractometric sensitivity," *Opt. Exp.*, vol. 23, no. 3, Feb. 2015, Art. no. 2918.

[36] T. Guo *et al.*, "Highly sensitive detection of urinary protein variations using tilted fiber grating sensors with plasmonic nanocoatings," *Biosens. Bioelectron.*, vol. 78, pp. 221–228, Apr. 2016.

[37] M. Loyez, M. Lobry, R. Wattiez, and C. Caucheteur, "Optical fiber gratings immunoassays," *Sensors*, vol. 19, no. 11, Jun. 2019, Art. no. 2595.

[38] M. Lobry, K. Chah, M. Loyez, D. Kinet, and C. Caucheteur, "Refractometric sensing with plasmonic tilted Bragg gratings in different fiber types," *Opt. Sens. Detection VI*, Apr., 2020, Art. no. 104.

[39] Y. Shevchenko, T. J. Francis, D. A. D. Blair, R. Walsh, M. C. DeRosa, and J. Albert, "In Situ biosensing with a surface plasmon resonance fiber grating aptasensor," *Anal. Chem.*, vol. 83, no. 18, pp. 7027–7034, Sep. 2011.

[40] X. Qiu, X. Chen, F. Liu, B.-O. Guan, and T. Guo, "Plasmonic fiber-optic refractometers based on a high Q-factor amplitude interrogation," *IEEE Sens. J.*, vol. 16, no. 15, pp. 5974–5978, Aug. 2016.

[41] M. Lobry *et al.*, "HER2 biosensing through SPR-envelope tracking in plasmonic optical fiber gratings," *Biomed. Opt. Exp.*, vol. 11, no. 9, Sep. 2020, Art. no. 4862.

[42] W. C. Wong *et al.*, "Photonic crystal fiber surface plasmon resonance biosensor based on protein g immobilization," *IEEE J. Sel. Topics Quantum Electron.*, vol. 19, no. 3, pp. 4602107–4602107, May 2013.

[43] Y. Liu *et al.*, "Ultra-high sensitivity plasmonic sensor based on D-shaped photonic crystal fiber with offset-core," *Optik (Stuttg),* vol. 221, Art. no. 165309, 2020.
[44] T. Geernaert *et al.*, "Bragg grating inscription in GeO-doped microstructured optical fibers," *J. Lightw. Technol.*, vol. 28, no. 10, pp. 1459–1467, May 2010.
[45] "Northlab photonics," Accessed: Nov. 14, 2021. [Online]. Available: https://www.northlabphotonics.com/
[46] "Ibsen photonics," Accessed: Nov. 14, 2021. [Online]. Available: https://ibsen.com/
[47] "Alcoa fujikura ltd.," Accessed: Nov. 14, 2021. [Online]. Available: https://www.aflglobal.com/
[48] T. Baghdasaryan, T. Geernaert, H. Thienpont, and F. Berghmans, "Numerical modeling of femtosecond laser inscribed IR gratings in photonic crystal fibers," *Opt. Exp.*, vol. 23, no. 2, Jan. 2015, Art. no. 709.
[49] F. Berghmans, T. Geernaert, T. Baghdasaryan, and H. Thienpont, "Challenges in the fabrication of fibre Bragg gratings in silica and polymer microstructured optical fibres," *Laser Photon. Rev.*, vol. 8, no. 1, pp. 27–52, Jan. 2014.
[50] K. Chah, V. Voisin, D. Kinet, and C. Caucheteur, "Surface plasmon resonance in eccentric femtosecond-laser-induced fiber Bragg gratings," *Opt. Lett.*, vol. 39, no. 24, Dec. 2014, Art. no. 6887.
[51] K. Chah, D. Kinet, and C. Caucheteur, "Negative axial strain sensitivity in gold-coated eccentric fiber Bragg gratings," *Sci. Rep.*, vol. 6, no. 1, Dec. 2016, Art. no. 38042.
[52] T. Baghdasaryan, T. Geernaert, P. Mergo, F. Berghmans, and H. Thienpont, "Transverse propagation of ultraviolet and infrared femtosecond laser pulses in photonic crystal fibers," *Photon. Lett. Pol.*, vol. 4, no. 2, pp. 72–74, Jun. 2012.
[53] J. C. Flanagan, R. Amezcua, F. Poletti, J. R. Hayes, N. G. R. Broderick, and D. J. Richardson, "The effect of periodicity on the defect modes of large mode area microstructured fibers," *Opt. Exp.*, vol. 16, no. 23, Nov. 2008, Art. no. 18631.
[54] F. Brechet, J. Marcou, D. Pagnoux, and P. Roy, "Complete analysis of the characteristics of propagation into photonic crystal fibers, by the finite element method," *Opt. Fiber Technol.*, vol. 6, no. 2, pp. 181–191, Apr. 2000.
[55] N. A. Mortensen, J. R. Folkenberg, M. D. Nielsen, and K. P. Hansen, "Modal cutoff and the V parameter in photonic crystal fibers," *Opt. Lett.*, vol. 28, no. 20, Oct. 2003, Art. no. 1879.
[56] C. Caucheteur, M. Loyez, Á. González-Vila, and R. Wattiez, "Evaluation of gold layer configuration for plasmonic fiber grating biosensors," *Opt. Exp.*, vol. 26, no. 18, Sep. 2018, Art. no. 24154.
[57] M. Daimon and A. Masumura, "Measurement of the refractive index of distilled water from the near-infrared region to the ultraviolet region," *Appl. Opt.*, vol. 46, no. 18, pp. 3811, Jun. 2007.
[58] L. Rindorf and O. Bang, "Sensitivity of photonic crystal fiber grating sensors: Biosensing, refractive index, strain, and temperature sensing," *J. Opt. Soc. Amer. B*, vol. 25, no. 3, Mar. 2008, Art. no. 310.
[59] L.-Y. Shao, Y. Shevchenko, and J. Albert, "Intrinsic temperature sensitivity of tilted fiber Bragg grating based surface plasmon resonance sensors," *Opt. Exp.*, vol. 18, no. 11, May 2010, Art. no. 11464.
[60] Y. H. Kim *et al.*, "Thermo-optic coefficient measurement of liquids based on simultaneous temperature and refractive index sensing capability of a two-mode fiber interferometric probe," *Opt. Exp.*, vol. 20, no. 21, Oct. 2012, Art. no. 23744.
[61] Y. Zhang *et al.*, "A novel fiber optic surface plasmon resonance biosensors with special boronic acid derivative to detect glycoprotein," *Sensors*, vol. 17, no. 10, Oct. 2017, Art. no. 2259.
[62] G. Rajan, "Basics of OTDR," in *Optical Fiber Sensors: Advanced Techniques and Applications*, 1st ed. Boca Raton, FL, USA: CRC Press, 2015, pp. 320–321.
[63] J. U. Thomas *et al.*, "Cladding mode coupling in highly localized fiber Bragg gratings II: Complete vectorial analysis," *Opt. Exp.*, vol. 20, no. 19, Sep. 2012, Art. no. 21434.
[64] C. Trono, F. Baldini, M. Brenci, F. Chiavaioli, and M. Mugnaini, "Flow cell for strain- and temperature-compensated refractive index measurements by means of cascaded optical fibre long period and Bragg gratings," *Meas. Sci. Technol.*, vol. 22, no. 7, Jul. 2011, Art. no. 075204.
[65] H. Chikh-Bled, M. Debbal, M. Chikh-Bled, C.-E. Ouadah, V. Calero-Vila, and M. Bouregaa, "Refractive index sensor in eccentric fiber Bragg gratings using a point-by-point IR femtosecond laser," *Appl. Opt.*, vol. 58, no. 3, Jan. 2019, Art. no. 528.
[66] Á. González-Vila, A. Ioannou, M. Loyez, M. Debliquy, D. Lahem, and C. Caucheteur, "Surface plasmon resonance sensing in gaseous media with optical fiber gratings," *Opt. Lett.*, vol. 43, no. 10, May 2018, Art. no. 2308.
[67] M. D. Baiad and R. Kashyap, "Concatenation of surface plasmon resonance sensors in a single optical fiber using tilted fiber Bragg gratings," *Opt. Lett.*, vol. 40, no. 1, Jan. 2015, Art. no. 115.